This is a repository copy of *Nonlinear spin filter for nonmagnetic materials at zero magnetic field*.

White Rose Research Online URL for this paper:
https://eprints.whiterose.ac.uk/198072/

Version: Accepted Version

Article:

Marcellina, E., Srinivasan, A. orcid.org/0000-0003-3003-7288, Nichele, F. et al. (5 more authors) (2020) Nonlinear spin filter for nonmagnetic materials at zero magnetic field. Physical Review B, 102 (14). 140406. ISSN 2469-9950

https://doi.org/10.1103/physrevb.102.140406

© 2020 American Physical Society. This is an author-produced version of a paper subsequently published in Physical Review B. Uploaded in accordance with the publisher's self-archiving policy. E. Marcellina, A. Srinivasan, F. Nichele, P. Stano, D. A. Ritchie, I. Farrer, Dimitrie Culcer, and A. R. Hamilton. Phys. Rev. B 102, 140406(R) – Published 21 October 2020

Reuse

Items deposited in White Rose Research Online are protected by copyright, with all rights reserved unless indicated otherwise. They may be downloaded and/or printed for private study, or other acts as permitted by national copyright laws. The publisher or other rights holders may allow further reproduction and re-use of the full text version. This is indicated by the licence information on the White Rose Research Online record for the item.

Takedown

If you consider content in White Rose Research Online to be in breach of UK law, please notify us by emailing eprints@whiterose.ac.uk including the URL of the record and the reason for the withdrawal request.

eprints@whiterose.ac.uk
https://eprints.whiterose.ac.uk/

arXiv:1907.01312v3 [cond-mat.mes-hall] 22 Oct 2020

Non-linear spin filter for non-magnetic materials at zero magnetic field

E. Marcellina,[1,*] A. Srinivasan,[1] F. Nichele,[2] P. Stano,[3,4,5] D. A. Ritchie,[6] I. Farrer,[6] Dimitrie Culcer,[1] and A. R. Hamilton[1]

[1] *School of Physics, The University of New South Wales, Sydney, Australia*
[2] *IBM Research - Zurich, Säumerstrasse 4, 8803 Rüschlikon, Switzerland*
[3] *RIKEN Center for Emergent Matter Science (CEMS), Wako, Saitama 351-0198, Japan*
[4] *Department of Applied Physics, School of Engineering, University of Tokyo, 7-3-1 Hongo, Bunkyo-ku, Tokyo 113-8656, Japan*
[5] *Institute of Physics, Slovak Academy of Sciences, 845 11 Bratislava, Slovakia*
[6] *Cavendish Laboratory, University of Cambridge, J. J. Thomson Avenue, Cambridge CB3 0HE, United Kingdom*

(Dated: October 23, 2020)

The ability to convert spin accumulation to charge currents is essential for applications in spintronics. In semiconductors, spin-to-charge conversion is typically achieved using the inverse spin Hall effect or using a large magnetic field. Here we demonstrate a general method that exploits the non-linear interactions between spin and charge currents to perform all-electrical, rapid and non-invasive detection of spin accumulation without the need for a magnetic field. We demonstrate the operation of this technique with ballistic GaAs holes as a model system with strong spin-orbit coupling, in which a quantum point contact provides the non-linear energy filter. This approach is generally applicable to electron and hole systems with strong spin orbit coupling.

Introduction. Spintronics is a technology that uses the spin degree of freedom to manipulate information [1, 2]. A key challenge in spintronics is the generation and detection of spin accumulation [3]. In semiconductors, spin accumulation is typically generated by optical excitations [4–8] or the intrinsic spin Hall effect [9–12], whilst spin-to-charge conversion (i.e. spin accumulation translating into a charge current or voltage) is achieved through the inverse spin Hall effect [9–11]. However, generating/detecting spin accumulation optically or via the spin Hall effect-inverse spin Hall effect pair is challenging for strongly spin-orbit coupled mesoscopic systems with short spin relaxation time and spin diffusion lengths.

Here we adapt the concept of a spin filter, i.e. a device that separates spin species based on their energies, for detecting spin accumulation in strongly spin-orbit coupled mesoscopic systems. The first spin filter was developed by Stern and Gerlach who used an inhomogenous magnetic field to spatially separate electrons with different spins [13]. Spin filters have also been realized in the solid state using spin-dependent transport in mesoscopic devices [14, 15]. These techniques allow a spin current to be converted into a charge current, which is then detected as a voltage signal that depends on the applied magnetic field. Unfortunately, these linear techniques require a large magnetic field, which is impractical and can change the spin signal being probed. In this work, we demonstrate a non-linear technique that requires no magnetic field, and allows fast detection of spin accumulation.

We use GaAs holes as a model system for strongly spin-orbit coupled systems with short spin relaxation time ($<$ 100 fs) [16] and spin diffusion length much shorter than the typical device dimensions ($\sim 100 - 1000$ nm, see also Sec. S2 of the Supplementary Material). Semiconductor holes have recently attracted great interest in semiconductor spintronics due to their exceptionally strong spin-orbit interaction [17–24]. The spin accumulation in strongly spin-orbit coupled ballistic mesoscopic systems is generated as follows. In mesoscopic systems with strong spin-orbit interaction, charge currents are generally accompanied by spin currents [25–29]. When the spin-orbit length is much shorter than both the device dimensions and mean free path, the spin precesses around randomly oriented spin-orbit fields throughout the sample region, giving rise to spin currents with a non-zero average [27]. Consequently, different spin species can have different chemical potentials, which give rise to a net spin accumulation whose amount and distribution depend on the sample geometry as well as the strength and form of the spin-orbit interaction. The spin accumulation adjacent to the energy barrier can then be detected through a voltage signal containing contributions linear and non-linear in spin accumulation.

This paper is laid out as follows. We first demonstrate spin-to-charge conversion in the linear regime using an in-plane magnetic field. We then show spin-to-charge conversion in the non-linear regime and confirm that it works even at zero magnetic field, so that is all-electrical and works much faster than linear spin-to-charge conversion. Our method can be generalized for any strongly spin-orbit coupled material such as GaSb, InAs, transition metal dichalcogenides, as well as topological insulators, since non-linear spin-to-charge conversion only requires a finite spin accumulation, regardless of the spin orientation, and an energy barrier. Furthermore, the rapidness of non-linear spin-to-charge conversion enables detection of spin orientation with radio-frequency techniques down

* Present address: School of Physical and Mathematical Sciences, Nanyang Technological University, 21 Nanyang Link, Singapore 637371. Email: emarcellina@ntu.edu.sg

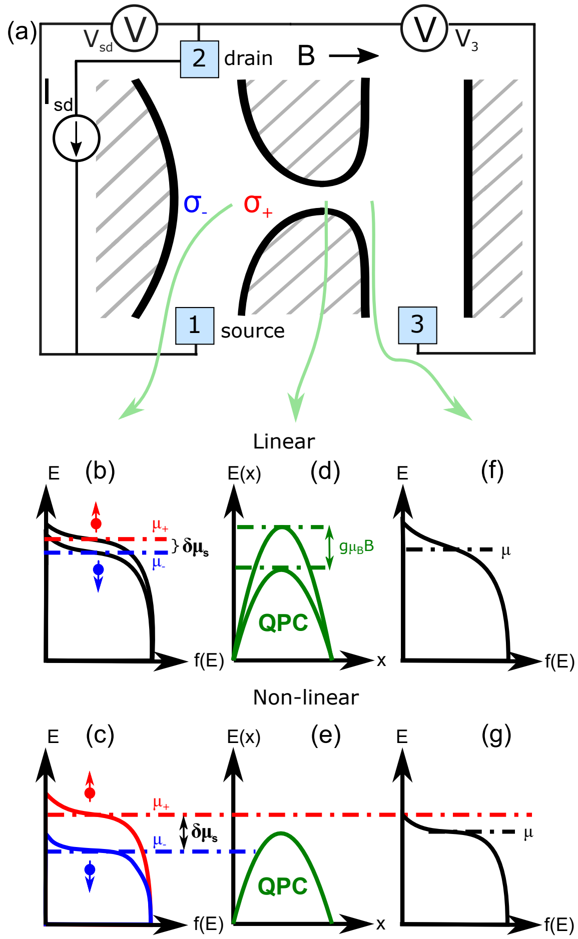

FIG. 1. (a) A schematic of the experimental setup. A current $I_{\rm sd}$ flows between terminals 1 and 2, resulting in a voltage difference $V_{\rm sd}$ across the drive channel. (b), (c) Near the quantum point contact (QPC), opposite spin orientations σ_+ and σ_- accumulate on opposite sides of the drive channel. The QPC acts as an energy filter: Spin-to-charge conversion occurs due to the difference in the transmission probability through the QPC between each spin species. In the linear regime (d), this difference arises from a different kinetic energy caused by, for instance, a Zeeman interaction. (e) In the non-linear regime, the different local chemical potentials for σ_+ and σ_- give rise to different transmission probabilities. In both (f) linear and (g) non-linear cases, spin-polarized holes accumulate after passing through the QPC, resulting in a voltage V_3 between terminals 2 and 3. Note that the schematics in (a)-(g) are not to scale.

to 1 ns [30].

Experimental concept. We use a three-terminal geometry with a quantum point contact (QPC) as an energy-selective barrier (Fig. 1a). Passing a current $I_{\rm sd}$ in the drive channel between terminals 1 and 2 results in a voltage difference $V_{\rm sd}$ and a net non-equilibrium spin accumulation $\delta\mu_s$: Spins with orientation σ_+ have a higher chemical potential (of $\delta\mu_s$) than σ_- (Figs. 1b and c). The kink in the drive channel helps direct the spin accumulation towards the QPC [31]. Spin-to-charge conversion occurs if one spin species has a higher transmission probability $T(E)$ through the QPC than the other. In the linear regime, the difference in the transmission probability originates from the difference in the hole's kinetic energy due to an in-plane Zeeman interaction (Fig. 1d). However, in the non-linear regime, the energy dependence of the transmission probability $T(E)$ through the barrier causes the σ_+ spins to have a higher transmission probability through the QPC (Fig. 1e) than σ_- even at zero field. In both the linear and non-linear regimes, the charge current through the QPC (Figs. 1f and g) causes a restoring voltage V_3 to maintain zero net charge current through the QPC with terminal 3 set as a floating probe. While the drive current $I_{\rm sd}$ oscillates at a frequency ω, the linear and non-linear signals oscillate at the first and second harmonics of V_3, i.e. $V_3(\omega)$ and $V_3(2\omega)$ respectively.

Theoretical analysis. Using the transmission probability $T(E) \equiv T(E,B)$ for a QPC [33] (see also Sec. S1 of the Supplementary Material [34]), in the linear regime, the spin signal is proportional to the Zeeman splitting of the one-dimensional subbands. This gives rise to a three-terminal voltage $V_3(\omega) \equiv V_3(\omega,B)$ asymmetric in B. The asymmetry $\partial_B V_3(\omega)|_{B=0}$ is [32]:

$$\partial_B V_3(\omega)|_{B=0} = -\frac{\sigma g \mu_B}{2}\left[\frac{2e}{h}\int dE\,(-\partial_E f(E))\,\partial_E T(E)\right]\delta\mu_s, \tag{1}$$

where σ is the sign of the spin accumulation, g is the in-plane $g-$factor, μ_B is the Bohr magneton, and $f(E)$ is the Fermi-Dirac distribution. Eq. (1) allows one to quantify the spin accumulation from the voltage asymmetry. The spin current through the QPC is [15, 28]

$$I_{\rm spin,linear} \simeq \frac{2\hbar\Omega_{\rm qpc}}{\pi g \mu_B}\frac{e^2}{h}\partial_B V_3(\omega)|_{B=0}, \tag{2}$$

where $\hbar\Omega_{\rm qpc}$ is the QPC saddle potential curvature [33].

In the non-linear regime, the difference in the transmission probability across the QPC is proportional to $\delta\mu_s$. Thus, the non-linear component of the spin signal V_3 is quadratic in $\delta\mu_s$:

$$V_3(2\omega) = \frac{1}{2}\left[\frac{e}{h}\int dE\,(-\partial_E f(E))\,\partial_E T(E)\right](\delta\mu_s)^2. \tag{3}$$

Given that $V_3(2\omega)$ is independent of the sign of $\delta\mu_s$, it is also symmetric in B.

Besides quantifying the spin current and accumulation, Eqs. (1)-(3) allow us to verify the spin origin of $V_3(\omega)$ and $V_3(2\omega)$ via their dependence on the QPC gate voltage $V_{\rm qpc}$, B, and $I_{\rm sd}$. Furthermore, since $\partial_E T(E)$ [Eqs. (1) and (3)] correlates with the QPC transconductance $\partial G_{\rm qpc}/\partial V_{\rm qpc}$, we expect maximal (no) spin signals when $\partial G_{\rm qpc}/\partial V_{\rm qpc}$ is maximal (minimal), where $G_{\rm qpc}$ is the QPC conductance.

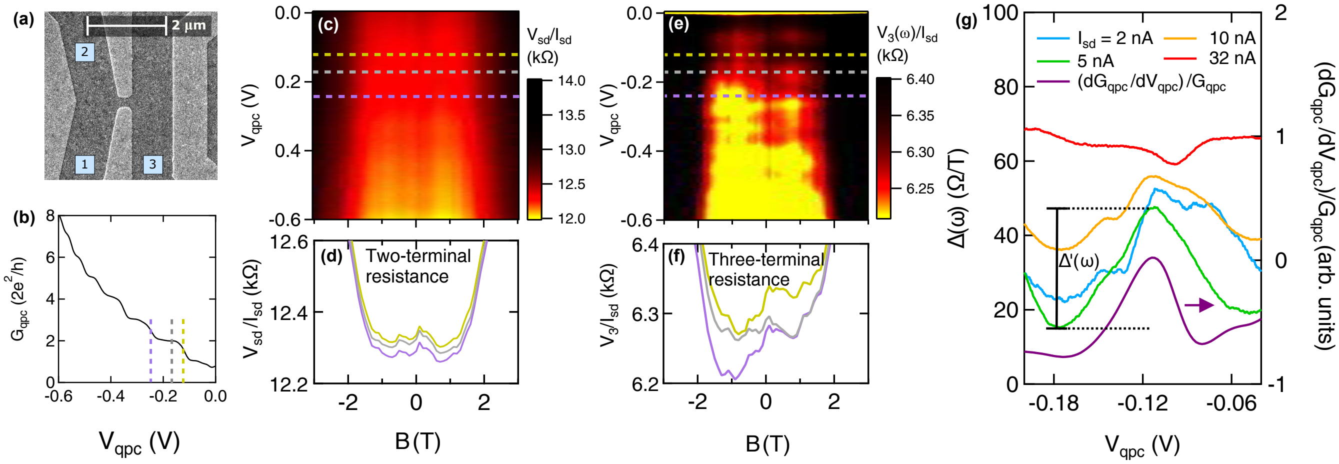

FIG. 2. Device image and linear spin-to-charge conversion. (a) A scanning electron microscope image of the device. Light gray regions denote the surface gates, dark gray regions represent the AlGaAs/GaAs heterostructure, while light blue squares depict terminals 1-3. (b) QPC conductance versus QPC gate voltage $V_{\rm qpc}$. The dashed lines denote the second and third conductance risers as well as the second conductance plateau. (c) Color map of the two-terminal resistance $V_{\rm sd}/I_{\rm sd}$ across the channel as a function of $V_{\rm qpc}$ and B, showing a symmetric dependence on B. (d) Line cuts of $V_{\rm sd}/I_{\rm sd}$ from (c) along the second and third QPC conductance risers, as well as along the middle of the second conductance plateau. (e) Color map of the three-terminal resistance $V_3(\omega)/I_{\rm sd}$ as a function of $V_{\rm qpc}$ and B. Its asymmetry in B indicates a spin accumulation. (f) Line cuts of $V_3(\omega)/I_{\rm sd}$ from (e) along the second and third QPC conductance risers, as well as along the middle of the second conductance plateau. The asymmetry of $V_3(\omega)/I_{\rm sd}$ in B is present at a QPC conductance riser but absent at a plateau. (g) The asymmetry $\Delta(\omega) \equiv (\partial V_3/\partial B)|_{B=0}/I_{\rm sd}$ of $V_3(\omega)/I_{\rm sd}$ as a function of $V_{\rm qpc}$ around the second riser at different $I_{\rm sd}$. The asymmetry of $V_3(\omega)/I_{\rm sd}$ persists up to $I_{\rm sd} = 10$ nA, but becomes hard to correlate to the transconductance at 32 nA. The $\Delta(\omega)$ traces are offset by 25 Ω/T for clarity. The quantity $\Delta'(\omega)$ measures the amplitude of the asymmetry $\Delta(\omega)$ relative to the background.

Methods. An image of the device is shown in Fig. 2a. The device is made from an AlGaAs/GaAs heterostructure grown on a (100) GaAs substrate. For the measurements presented here, the two-dimensional hole density is $p = 2 \times 10^{11}$ cm^{-2}, corresponding to a Fermi wavelength $\lambda_F = 56$ nm, a spin-orbit length $l_{\rm SO} = 35$ nm, and a mobility $\mu = 550,000$ cm^2 V^{-1} s^{-1} (see Sec. S2 of the Supplementary Material [34]). Surface gates define a conducting region in the shape of a 'K', with length 4 μm and width 1 μm, whilst the QPC is 370 nm wide and 210 nm long. When the 'K-bar' is defined, the conducting channel in the region is one-dimensional and the transport is ballistic with a mean free path of 4 μm (see Sec. S3 of the Supplementary Material [34] for details). All measurements were performed in a dilution fridge using standard lock-in techniques with $\omega = 7$ Hz.

We send a current $I_{\rm sd}$ through the drive channel, and measure the resulting two-terminal $V_{\rm sd} \equiv V_1 - V_2$ and three-terminal voltages $V_3(\omega)$ between terminals 2 and 3 (see also Fig. 1). Unless otherwise stated, $I_{\rm sd}$ is kept at 5 nA. Throughout this work, we concentrate our analysis on the second subband. While the first subband is affected by the "0.7 feature" [35–39], the spin signal is small for higher subbands ($N_{\rm qpc} > 3$): The conductance quantization is progressively worse for these subbands, diminishing the spin-to-charge conversion efficiency. Fig. 2b shows how the QPC conductance is tuned by the QPC gate voltage. The two outer dashed lines mark the second and third conductance risers, where the spin-to-charge conversion should be most pronounced. The middle dashed line locates the second QPC plateau, where the spin-to-charge conversion should be suppressed. Fig. 2c shows the two-terminal resistance $V_{\rm sd}/I_{\rm sd}$ across the drive channel as a function of $V_{\rm qpc}$ and B. As expected from the Onsager reciprocity relation for electrical current in two-terminal systems, $V_{\rm sd}/I_{\rm sd}$ is approximately symmetric in B (the QPC is a small perturbation to the drive channel, see Fig. S4 of the Supplementary Material [34]). Fig. 2d shows line cuts of Fig. 2c at the second and third QPC conductance risers and at the second QPC conductance plateau, confirming that $V_{\rm sd}$ is approximately symmetric in B regardless of $V_{\rm qpc}$.

Linear spin-to-charge conversion. We now examine the linear three-terminal voltage $V_3(\omega)$. Fig. 2e shows $V_3(\omega)/I_{\rm sd}$ as a function of $V_{\rm qpc}$ and B, demonstrating that $V_3(\omega)$ is generally asymmetric in B. The line cuts of Fig. 2e shown in Fig. 2f reveal that $V_3(\omega)/I_{\rm sd}$ is asymmetric in B on the second and third QPC conductance risers, but almost symmetric on the middle of the second conductance plateau. This is a crucial observation for the linear spin-to-charge conversion: The asymmetry of V_3 with B is expected only if the spin accumulation is present and the QPC transmission is spin-(Zeeman energy) sensitive. At the QPC conductance plateau, although the spin current is still flowing through the QPC, it is not converted to a charge voltage. The asymmetry in $V_3(\omega)$ as a function of B cannot be due to a Hall voltage as the sample was oriented to within $\pm 0.01°$ with

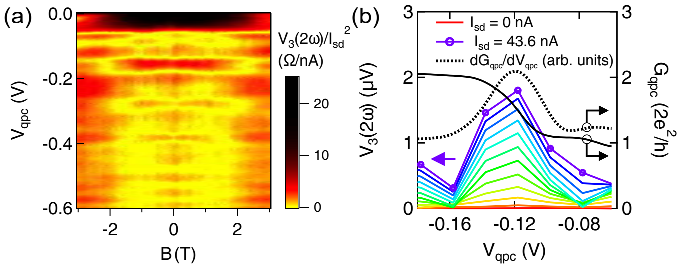

FIG. 3. (a) The non-linear resistance $V_3(2\omega)/I_{sd}^2$ as a function of V_{qpc} and B. (b) The non-linear voltage $V_3(2\omega)$ as a function of V_{qpc} for various I_{sd} is proportional to the QPC transconductance at $B = 0$ T.

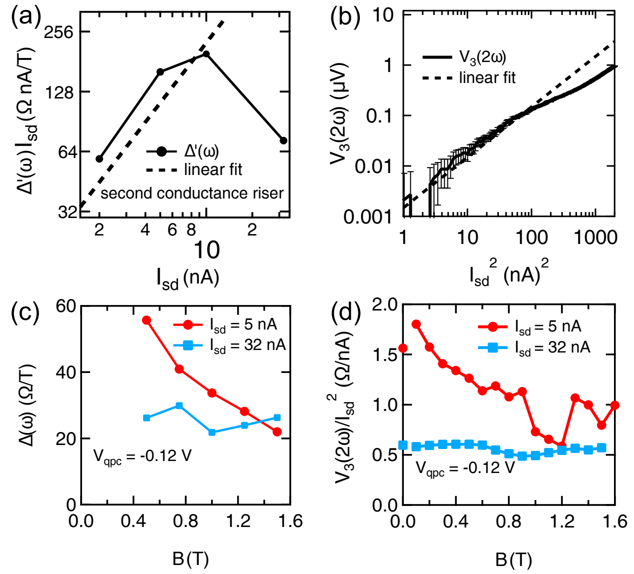

FIG. 4. (a) The amplitude $\Delta'(\omega)I_{sd}$ of the linear signal relative to the background, which is obtained by subtracting the lowest adjacent $\Delta(\omega)$ minimum (see also Fig. 2g) from $\Delta(\omega)$ at the second QPC riser. (b) $V_3(2\omega)$ versus I_{sd} at $B = 0$. The dashed lines in (a) and (b) are guides to the eye, suggesting that the linear and non-linear spin signals saturate at ∼5-10 nA. (c) The asymmetry $\Delta(\omega)$ of the linear signal and (d) the non-linear resistance $V_3(2\omega)/I_{sd}^2$ versus B. (c) and (d) show that at low excitation currents (e.g. $I_{sd} = 5$ nA), the spin signal gradually decreases as a function of B, whereas at high excitation currents (e.g. $I_{sd} = 32$ nA), it is almost unaffected by B. The difference in the $B-$dependence of the low and high I_{sd} signals suggests that at low I_{sd} the three-terminal voltages are of spin origin.

respect to the magnetic field [40], so that the out-of-plane magnetic field is always < 0.5 mT.

We next quantify the spin accumulation, spin current and the spin-to-charge conversion efficiency. Fig. 2g shows the asymmetry $\Delta(\omega) \equiv \frac{1}{I_{sd}} \frac{\partial V_3(\omega)}{\partial B}\Big|_{B=0} \propto I_{spin,linear}$ of the three-terminal resistance at $I_{sd} = 2,\ 5,\ 10,\ 32$ nA as a function of V_{qpc}. The asymmetry $\Delta(\omega)$ is obtained by performing a linear fit of $V_3(\omega)$ against B between -1 T $\leq B \leq 1$ T in Fig. 2g [41]. There is a clear correlation between $\Delta(\omega)$ and $\partial_{V_{qpc}} G_{qpc}/G_{qpc}$, which indicates linear spin-to-charge conversion (Eq. 1) for currents up to $I_{sd} = 10$ nA. The spin signal is suppressed at large I_{sd} (e.g. at $I_{sd} = 32$ nA), possibly due to averaging out of spin accumulations at different energies [15].

Using the results in Fig. 2g and experimental parameters $I_{sd} = 5$ nA, $g = 0.38 \pm 0.01$, $\hbar\Omega_{qpc} = (0.17 \pm 0.01)$ meV (see Sec. S3 of the Supplementary Material), $\Delta(\omega) = 40$ Ω/T, $N_{drive} = 14$ (see Sec. S4 of the Supplementary Material [41]) and $N_{qpc} = 1.5$, we find that the spin accumulation is $\delta\mu_s = 1$ μeV (Eq. S7) while the spin current is $I_{spin,linear} = 37$ pA (Eq. 2). The spin Hall angle [15], which measures the spin-to-charge conversion efficiency, is $\Theta \equiv (I_{spin,linear}/N_{qpc})/(I_{sd}/N_{drive}) = 6.8\%$. While our spin Hall angle falls within the range of previously reported values [15, 42–44], caution must be exercised in the comparison since Θ is not only determined by the material but also the device details.

Non-linear spin-to-charge conversion. Now that we have established evidence for spin-to-charge conversion in the linear regime, we show that it also occurs in the non-linear regime. As before, we evaluate the dependence of the non-linear signal $V_3(2\omega)$ on B, V_{qpc}, and I_{sd}. Fig. 3a shows a color map of the non-linear resistance $V_3(2\omega)/I_{sd}^2$ as a function of B and V_{qpc}. The non-linear signal $V_3(2\omega)$ is symmetric in B, contrasting with the linear signal $V_3(\omega)$ (Fig. 2e), and in line with Eq. (3). Next, we examine the dependence of V_{qpc} at $0 \leq I_{sd} \leq 44.1$ nA at $B = 0$ T (Fig. 3b). The peak in the non-linear signal coincides with the QPC transconductance since $\partial_E T(E)$ is maximal at $T(E) = 1/2$ when $B = 0$ T, consistent with Eq. (3).

We next compare the linear and non-linear signals. Fig. 4a shows the amplitude $\Delta'(\omega)$ of the linear signal relative to the background, i.e. the value of $\Delta(\omega)$ at the second subband subtracted by the lowest minimum (see Fig. 2g), against I_{sd}. The spin current is linear in I_{sd} (and hence $\delta\mu_s$) at low excitation currents ($I_{sd} \lesssim 5$ nA, see Fig. 4a). For comparison, Fig. 4b shows how $V_3(2\omega)$ varies with I_{sd}. We find that the non-linear voltage is proportional to I_{sd}^2 for $I_{sd} \lesssim 7$ nA. While there is a possibility that Joule heating, which causes thermopower [45, 46], could contribute to the second-harmonic response, the fact that both the linear and non-linear signals saturate at similar I_{sd} (≈ 5 nA and ≈ 7 nA for the linear and non-linear signals, respectively) suggests that they are of a spin origin.

To further verify the spin origin of the signals, we consider their dependence on B at low ($I_{sd} = 5$ nA) and high ($I_{sd} = 32$ nA) excitation currents. At low I_{sd} (Figs. 4a and b), both the linear (Fig. 4c, see also Sec. S5 of the Supplementary Material [41]) and non-linear signals (Fig. 4d) gradually decrease at $B \gtrsim 1.4$ T, suggesting that a strong magnetic field suppresses the spin accumulation. In contrast, for high I_{sd}, where the spin-to-charge conversion is inefficient [32], both the linear and non-linear signals are almost unaffected by the in-plane magnetic field (see also Sec. S6 of the Supplementary Material [41]). The consistency between the linear and non-linear signals confirms the reliability of non-linear spin-to-charge conversion. As non-linear spin-to-charge conversion requires no magnetic field (Figs. 3b and 4b), it allows a much faster detection of spin accumulation than linear spin-to-charge conversion [47].

Conclusions and outlook. Using ballistic mesoscopic GaAs holes as a model system, we demonstrate a new all-electrical non-linear technique for spin-to-charge conversion that does not require a magnetic field. We confirm the spin origin of the non-linear signals by calibrating them against linear spin-to-charge conversion. The non-linear spin detection technique allows much faster measurements than linear detection schemes, limited only by the bandwidth of the measurement circuit. Finally, we note that non-linear spin-to-charge conversion is very general: it only requires a spin accumulation regardless of its orientation and an adjacent energy-selective barrier. Our methods should be applicable in materials with very strong spin-orbit interaction such as GaSb, InAs, transition metal dichalcogenides, and topological materials, while its rapid speed will enable time resolved measurements of spin orientation to a 1 ns resolution using radio-frequency techniques.

Acknowledgment. The authors would like to thank Heiner Linke and I-Ju Chen for many enlightening discussions. This work was supported by the Australian Research Council under the Discovery Projects scheme and CE170100039. The device 27F8Q was fabricated using the facilities of the New South Wales 279 Node of the Australian National Fabrication Facility. F. Nichele acknowledges support from European Research Commission, grant number 804273.

[1] S. A. Wolf, D. D. Awschalom, R. A. Buhrman, J. M. Daughton, S. von Molnár, M. L. Roukes, A. Y. Chtchelkanova, and D. M. Treger, Science **294**, 1488 (2001).

[2] I. Žutić, J. Fabian, and S. Das Sarma, Rev. Mod. Phys. **76**, 323 (2004).

[3] W. Han, Y. Otani, and S. Maekawa, npj quantum mater. **3**, 1 (2018).

[4] N. P. Stern, S. Ghosh, G. Xiang, M. Zhu, N. Samarth, and D. D. Awschalom, Phys. Rev. Lett. **97**, 126603 (2006).

[5] H. J. Chang, T. W. Chen, J. W. Chen, W. C. Hong, W. C. Tsai, Y. F. Chen, and G. Y. Guo, Phys. Rev. Lett. **98**, 136403 (2007).

[6] S. Matsuzaka, Y. Ohno, and H. Ohno, Phys. Rev. B **80**, 241305(R) (2009).

[7] K. Ando, M. Morikawa, T. Trypiniotis, Y. Fujikawa, C. H. W. Barnes, and E. Saitoh, Appl. Phys. Lett. **86**, 082502 (2010).

[8] J. Wunderlich, B.-G. Park, A. C. Irvine, L. P. Zârbo, E. Rozkotová, P. Nemec, V. Novák, J. Sinova, and T. Jungwirth, Science **330**, 1801 (2010).

[9] C. Brüne, A. Roth, E. G. Novik, M. König, H. Buhmann, E. M. Hankiewicz, W. Hanke, and J. Sinova, Nat. Phys. **6**, 448 (2010).

[10] J. Balakrishnan, G. Kok Wai Koon, M. Jaiswal, A. H. Castro Neto, and B. Özyilmaz, Nat. Phys. **9**, 284 (2013).

[11] W. Y. Choi, H.-J. Kim, J. Chang, S. H. Han, H. C. Koo, and M. Johnson, Nature Nanotechnol. **10**, 666 (2015).

[12] F. Bottegoni, C. Zucchetti, S. Dal Conte, J. Frigerio, E. Carpene, C. Vergnaud, M. Jamet, G. Isella, F. Ciccacci, G. Cerullo, and M. Finazzi, Phys. Rev. Lett. **118**, 167402 (2017).

[13] W. Gerlach and O. Stern, Z. Phys. **9**, 349 (1922).

[14] S. Chesi, G. F. Giuliani, L. P. Rokhinson, L. N. Pfeiffer, and K. W. West Phys. Rev. Lett. **106**, 236601 (2011).

[15] F. Nichele, S. Hennel, P. Pietsch, W. Wegscheider, P. Stano, P. Jacquod, T. Ihn, and K. Ensslin, Phys. Rev. Lett. **114**, 206601 (2015).

[16] D. J. Hilton and C. L. Tang, Phys. Rev. Lett. **89**, 146601 (2002).

[17] G. Akhgar, O. Klochan, L. H. Willems van Beveren, M. T. Edmonds, F. Maier, B. J. Spencer, J. C. McCallum, L. Ley, A. R. Hamilton, and C. I. Pakes, Nano Letters **16**, 3768 (2016).

[18] D. Q. Wang, O. Klochan, J.-T. Hung, D. Culcer, I. Farrer, D. A. Ritchie, and A. R. Hamilton, Nano Lett. **16**, 7685 (2016).

[19] A. Srinivasan, D. S. Miserev, K. L. Hudson, O. Klochan, K. Muraki, Y. Hirayama, D. Reuter, A. D. Wieck, O. P. Sushkov, and A. R. Hamilton, Phys. Rev. Lett. **118**, 146801 (2017).

[20] E. Marcellina, A. Srinivasan, D. S. Miserev, A. F. Croxall, D. A. Ritchie, I. Farrer, O. P. Sushkov, D. Culcer, and A. R. Hamilton, Phys. Rev. Lett. **121**, 077701 (2018).

[21] N. W. Hendrickx, D. P. Franke, A. Sammak, M. Kouwenhoven, D. Sabbagh, L. Yeoh, R. Li, M. L. V. Tagliaferri, M. Virgillo, G. Capellini, G. Scappucci, and M. Veldhorst, Nat. Commun. **9**, 1 (2018).

[22] H. Watzinger, J. Kukučka, L. Vukušić, F. Gao, T. Wang, F. Schäffler, and G. Katsaros, Nat. Commun. **9**, 1 (2018).

[23] A. Crippa, R. Maurand, L. Bourdet, D. Kotekar-Patil, A. Amisse, X. Jehl, M. Sanquer, R. Laviéville, H. Bohuslavskyi, L. Hutin, S. Barraud, M. Vinet, Y.-M. Niquet, and S. De Franceschi, Phys. Rev. Lett. **120**, 137702 (2018).

[24] N. W. Hendrickx, D. P. Franke, A. Sammak, G. Scappucci, and M. Veldhorst, Nature **577**, 487 (2020).

[25] J. H. Bardarson, I. Adagideli, and P. Jacquod, Phys. Rev. Lett. **98**, 196601 (2007).

[26] J. J. Krich and B. I. Halperin, Phys. Rev. B **78**, 035338 (2008).

[27] I. Adagideli, P. Jacquod, M. Scheid, M. Duckheim, D. Loss, and K. Richter, Phys. Rev. Lett. **105**, 246807 (2010).

[28] P. Stano and P. Jacquod, Phys. Rev. Lett. **106**, 206602 (2011).

[29] J. G. G. S. Ramos, T. C. Vasconcelos, and A. L. R. Barbosa, J. Appl. Phys. **123**, 034304 (2018).

[30] L. J. Taskinen, R. P. Starrett, T. P. Martin, A. Micolich, A. R. Hamilton, M. Y. Simmons, D. A. Ritchie, and M. Pepper, Rev. Sci. Instrum. **79**, 123901 (2008).

[31] T. Benter, H. Lehmann, T. Matsuyama, W. Hansen, C. Heyn, U. Merkt, and J. Jacob, Appl. Phys. Lett. **102**, 212405 (2013).

[32] P. Stano, J. Fabian, and P. Jacquod, Phys. Rev. B **85**, 241301(R) (2012).

[33] M. Büttiker, Phys. Rev. B **41**, 7906 (1990).

[34] See the Supplementary Material at [URL] for additional details on theory of spin-to-charge conversion and device characterization.

[35] K. J. Thomas, J. T. Nicholls, M. Y. Simmons, M. Pepper, D. R. Mace, and D. A. Ritchie, Phys. Rev. Lett. **77**, 135 (1996).

[36] R. Danneau, O. Klochan, W. R. Clarke, L. H. Ho, A. P. Micolich, M. Y. Simmons, A. R. Hamilton, M. Pepper, and D. A. Ritchie, Phys. Rev. Lett. **100**, 016403 (2008).

[37] A. P. Micolich and U. Zülicke, J. Phys. Condens. Matter **23**, 362201 (2011).

[38] M. J. Iqbal, R. Levy, E. J. Koop, J. B. Dekker, J. P. de Jong, J. H. M. van der Velde, D. Reuter, A. D. Wieck, R. Aguado, Y. Meir, and C. H. van der Wal, Nature **501**, 79 (2013).

[39] F. Bauer, J. Heyder, E. Schubert, D. Borowsky, D. Taubert, B. Bruognolo, D. Schuh, W. Wegscheider, J. von Delft, and S. Ludwig, Nature **501**, 73 (2013).

[40] L. A. Yeoh, A. Srinivasan, T. P. Martin, O. Klochan, A. P. Micolich, and A. R. Hamilton, Rev. Sci. Instrum. **81**, 113905 (2010).

[41] The fitting ranges $|B| \leq 0.5, 0.75, 1, 1.25$ T give the same peak positions (see Sec. S5 of the Supplementary Material [41]).

[42] T. Jungwirth, J. Wunderlich, and K. Olejník, Nat. Mater. **11**, 382 (2012).

[43] J. Balakrishnan, G. K. W. Koon, A. Avsar, Y. Ho, J. H. Lee, M. Jaiswal, S.-J. Baeck, J.-H. Ahn, A. Ferreira, M. A. Cazalilla, A. H. Castro Neto, and B. Özyilmaz, Nat. Commun. **5**, 4748 (2014).

[44] J. Sinova, S. O. Valenzuela, J. Wunderlich, C. H. Back, and T. Jungwirth, Rev. Mod. Phys. **87**, 1213 (2015).

[45] N. J. Appleyard, J. T. Nicholls, M. Y. Simmons, W. R. Tribe, and M. Pepper, Phys. Rev. Lett. **81**, 3491 (1998).

[46] F. L. Bakker, A. Slachter, J. P. Adam, and B. J. van Wees, Phys. Rev. Lett. **105**, 136601 (2010).

[47] As an example, the linear spin-to-charge measurements in Fig. 2 took ~ 30 hours, as they needed data at both $+B$ and $-B$. The equivalent non-linear spin-to-charge conversion, which only involved measuring V_3 as a function of V_{qpc} at $B = 0$, took only ~ 10 minutes. .